Available online at www.sciencedirect.com

ScienceDirect

Procedia Structural Integrity 13 (2018) 601–606

Structural Integrity Procedia

www.elsevier.com/locate/procedia

ECF22 - Loading and Environmental effects on Structural Integrity

Influence of rebar design on mechanical behaviour of Tempcore steel

Hortigón B.[a]*, Ancio F.[a], Nieto-García E.J.[a], Herrera M.A.[a], Gallardo J.M.[b]

[a]*Escuela Politécnica Superior (Universidad de Sevilla), C/ Virgen de Africa,7,41011 Sevilla, España*
[b]*Escuela Técnica Superior de Ingeniería (Universidad de Sevilla), C/ Camino de los Descubrimientos s/n,41092 Sevilla, España*

Abstract

Tensile behaviour of metals beyond the ultimate tensile strength (UTS) must be considered to calculate toughness or absorbed energy till fracture. Structural steels, designed to withstand earthquakes, are the typical material where post necking behaviour can be of paramount importance. This paper deals with the tensile stress-strain behaviour of Tempcore Rebar, a specifically shaped structural steel. Helical, short ribs, formed by rolling, protrude from the cylindrical basic shape of the Rebar. This help in increasing concrete/steel adherence in reinforced structures. On the other hand, those ribs make it difficult to assess strain distribution in the necking area, according to well-known theories describing neck profile. New or modified experimental methods, along with new theoretical approaches must be developed to help in studying neck profile evolution and corresponding stresses in rebars. Advances in such methods and theories are presented in this paper along with comparison with Tempcore cylindrical bars necking behaviour. The effect of ribs is clearly identified.

Peer-review under responsibility of the ECF22 organizers.

Keywords: Tempcore, rebar, mechanical behaviour, necking, fracture.

Nomenclature*

E	Young's modulus (modulus of elasticity in tension)
F	Axial force (load)
S_o	Initial cross-sectional area
S	Instantaneous cross-sectional area
d_{out}	Outer diameter (determinated by longitudinal ribs)

* Hortigón B. Tel.: +34-954-552-828; fax: +34-954-552-828.
E-mail address: bhortigon@us.es

2452-3216
Peer-review under responsibility of the ECF22 organizers.
10.1016/j.prostr.2018.12.099

a	Instantaneous radius of minimum cross section
R	Instantaneous radius of curvature of the neck
$R_{p,0.2}$	Engineering yield strength computed to an offset strain of 0.2%
R_m	Engineering axial strength at maximum force (also referred to as ultimate tensile strength)
A	Engineering axial strain
A_{gt}	Engineering axial strain at R_m
A_t	Engineering axial strain at fracture
σ_z	True axial stress. For uniform strain, $\sigma_z = R\,(1+A)$
$\bar{\sigma}_z$	Average axial stress on minimum cross section
σ_{equ}	Equivalent axial stress on minimum cross section
ε_z	True axial strain. Can be computed as $\varepsilon_z = Ln(1+A)$
ε_{gt}	True axial strain corresponding to A_{gt}
ε_{equ}	Equivalent or logarithmic strain on minimum cross section

*Nomenclature follows the recommendations as per standard UNE EN ISO 6892-1:2016 (Aenor, 2016) and, when convenient, ASTM E6-09 (ASTM, 2009)

1. Introduction

Nowadays research on round tensile bars neck formation is still approached from the stress and strain distribution theory derived by Bridgman (1944). The hypothesis is based on an axial and mirror symmetry, in addition to a neck profile shaped like an arc of circle. Formulation to calculate equivalent stress and strain at minimum cross section result:

$$\varepsilon_{equ} = \ln \frac{S_0}{S} \tag{1}$$

$$\bar{\sigma}_z = \sigma_{equ}\left[(1+\frac{2R}{a}\ln\left(1+\frac{a}{2R}\right)\right] \tag{2}$$

From Eq. (2), σ_{equ} is computed by applying a correction coefficient to the average axial stress (F/S) as a function of the radius of curvature (R) and the radius of minimum cross section (a). Furthermore, alternative equations have been suggested by Davidenkov and Spiridnova (1946) and Eisenberg and Yen (1983).

To avoid measuring the instantaneous radius of curvature, Bridgman (1944) proposes a relationship between a/R and ε_{equ} through the equation:

$$\frac{a}{R} = \sqrt{\varepsilon_{equ} - 0.1} \tag{3}$$

Again, alternative equations have been proposed by Le Roy et al. (1981) and Bueno and Villegas (2011) for different materials.

Nevertheless, several authors (Donato and Ganharul (2013), Ganharul et al. (2012), La Rosa and Mirone (2003)) question Bridgman´s stress and strain distribution since it is only based on neck profile without taking into account the influence of the involved mechanisms.

The aim of this research is to validate Bridgman´s theory for two typologies of Tempcore steel bars, round and rebar. Experimental and simulation results are presented questioning the Bridgman proposition for rebar steel.

2. Materials and methods

Two batches of 14 mm nominal diameter, Tempcore steel bars have been tested. Both batches fulfill SD500 UNE-EN-10080:2006 standard (Aenor, 2006), except for the fact that one of them was finished round instead of ribbed. Equivalent diameter of rebar has been estimated by weighing a fixed length. Specific gravity of steel was taken as

78500 N/m^3. Tensile tests have been carried out according to standards UNE EN ISO 15630-1:2010 (Aenor, 2011) and UNE EN ISO 6892-1:2016 (Aenor, 2016). Strain rate was set to 0.167 mm.s^{-1}. Eight samples were tested for each batch. Average values of mechanical properties are shown in Table 1.

Table 1. Mechanical properties (average values)

Material	$R_{p,0.2}$ (MPa)	R_m (MPa)	$R_m/R_{p,0.2}$	A_{gt} (%)	A_t (%)	E (GPa)
TEMPCORE 1 (round)	518.70±7.18	627.26±2.85	1.21±0.02	10.6±0.3	18±1.6	195
TEMPCORE 2 (rebar)	521.46±11.13	647.19±1.37	1.24±0,03	15.6±0.8	21.9±1.2	200

Young modulus have been computed using a class 1 extensometer. High resolution images were obtained by the complete test, including the necking stage, in a synchronized mode to the force measurement. Neck geometry development has been assessed by selecting 12 images for each specimen, that were subsequently processed by an image processing software. For rebar specimens, the profile or silhouette of the longitudinal was recorded. For rebar steel, the results obtained using the described methodology was complemented with data of a post mortem 3D scan of the neck.

3. Results and discussion

Fig. 1a) shows the experimental results as graphs of engineering stress versus axial engineering strain of both steels. Very similar data are obtained for both materials during the homogeneous strain hardening stage. Nevertheless, a greater dispersion is found for engineering longitudinal strain values within the necking phase, i.e., standard deviation value for A_t is greater than for A_{gt} (see Table 1).

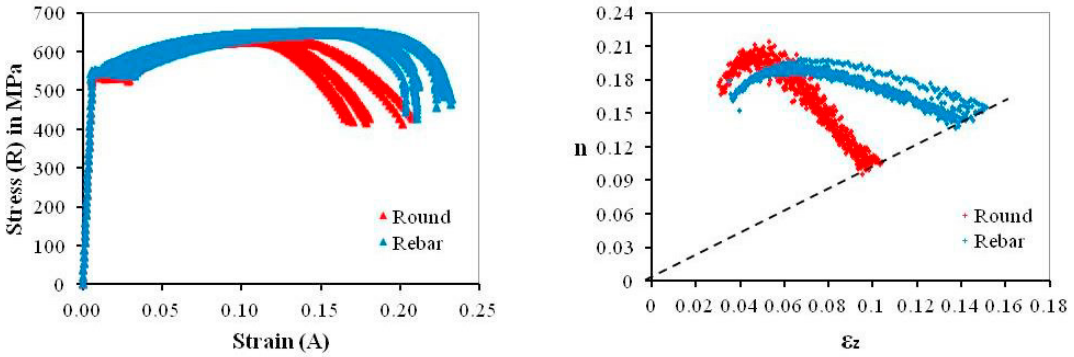

Fig. 1. a) Experimental results R vs A for both of tested steels, b) n vs ε_z according to Rastegari et al. (2015)

3.1. Homogeneous strain hardening behaviour

Average strain hardening exponent values computed after Hollomon and Jaffe (1945) are 0.176 for round specimens and 0.179 for rebar ones. For this average values, the criteria (n=ε_{gt}) as proposed by Considére (1885) cannot be validated. Nevertheless, a few authors (Rastegari et al. (2015), Fattah-alhosseini et al. (2016), Gashti et al. (2016)) consider that the value of n varies in the range analyzed, according to several mechanism activated in different strain levels. Rastegari et al. (2015) proposes the following equation to calculate instantaneous values of n, being the suffix i referred to experimental points:

$$n_i = \left(\varepsilon_{zi}\left(\sigma_{z(i+1)} - \sigma_{z(i-1)}\right)\right) \Big/ \left(\sigma_{zi}\left(\varepsilon_{z(i+1)} - \varepsilon_{z(i-1)}\right)\right) \tag{4}$$

The dependence of n_i with ε_{zi} up to ε_{gt}, is shown in Fig. 1b). Both materials show a similar behaviour: the value of n increases at the beginning of the plastic strain, but finally decreases on approaching ε_{gt}. As long as n_i remains high,

plastic strain is homogeneous and, consequently, necking onset is delayed. Finally, Considére (1885) criteria is fulfilled when $\varepsilon_z = \varepsilon_{gt}$.

3.2. Necking phase behaviour

Five specimens for each steel have been characterized to determine the necking behaviour. In the case of round bars, neck shape fits a toroidal surface with its axis aligned to the round bar axis, i.e., according to Bridgman's neck geometry (Bridgman, 1944). Therefore, cross section area on neck can be determine by image processing. On the other hand, for rebar steel, symmetry condition haven´t been validated. While a high fitting parameter ($R^2 \approx 0.98$ is obtained on adjusting an arc of circle to each side of the profile, Fig. 2a) shows both radius to be different (R_1 y R_2 are 84.15 y 72.6 mm, respectively). In addition, there is no coincidence of the minimum cross sections on both sides. Fig. 2b) shows the fracture of both specimens. Round bars form cup and cone surfaces while rebar specimens present a fracture in the direction of the transverse rib affected by necking. In fact, there occurs a localized plastic deformation at rib's root causing cracks nucleation (Fig. 3).

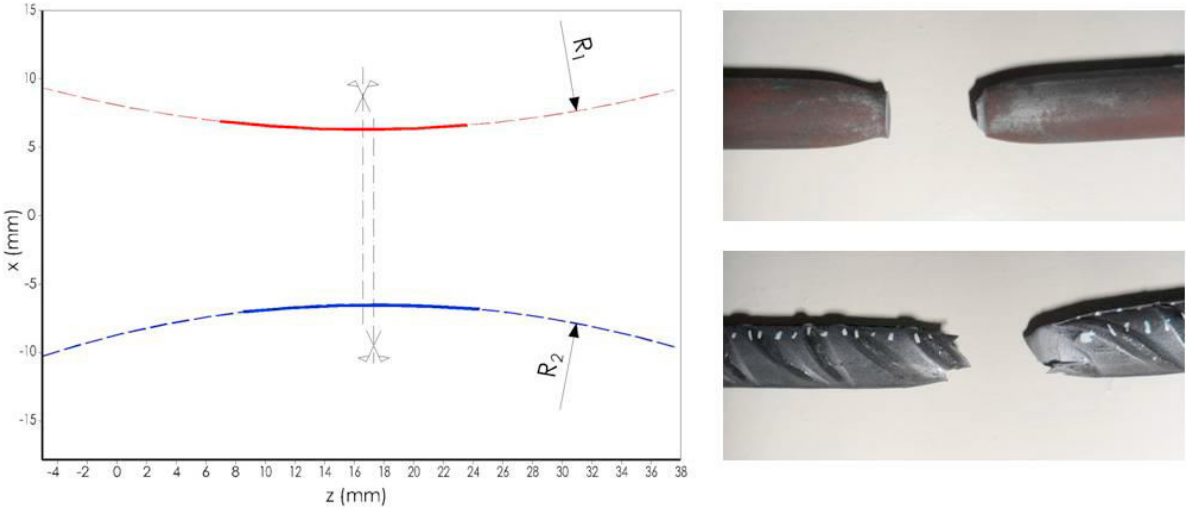

Fig. 2. a) Neck profile of a rebar specimen , b) fracture of round (right-up side) and rebar (right-down side) specimens

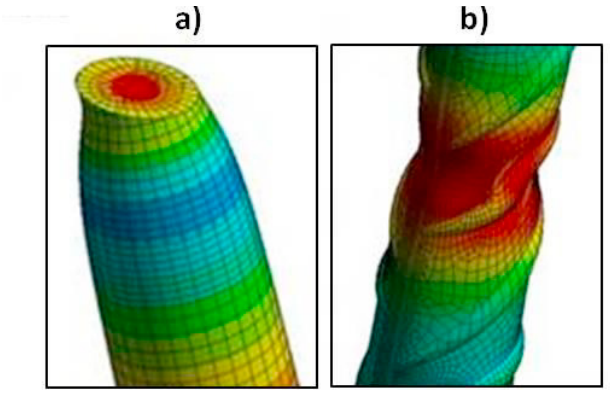

Fig. 3. Stress distribution on the neck obtained by FEM for round (a) and rebar (b) specimens

As a result, Bridgman´s methodology is not viable to rebar specimens necking research. Instead, a 3D assessment of neck evolution must be carried out. In this paper, only the neck shape at fracture has been determined by laser 3D scan and final reconstruction using the software Catia. Results obtained for instantaneous cross section (S) versus outer diameter (d_{out}) for one rebar specimen are shown in Fig. 4. Similar trend is observed along the upper and lower side of minimum cross section, with a high increase in the value of S on moving away from this one. Equation results:

$$S = 2.4858 d_{al}^3 - 95.451 d_{al}^2 + 1231.9 d_{al} - 5223.8 \quad (5)$$

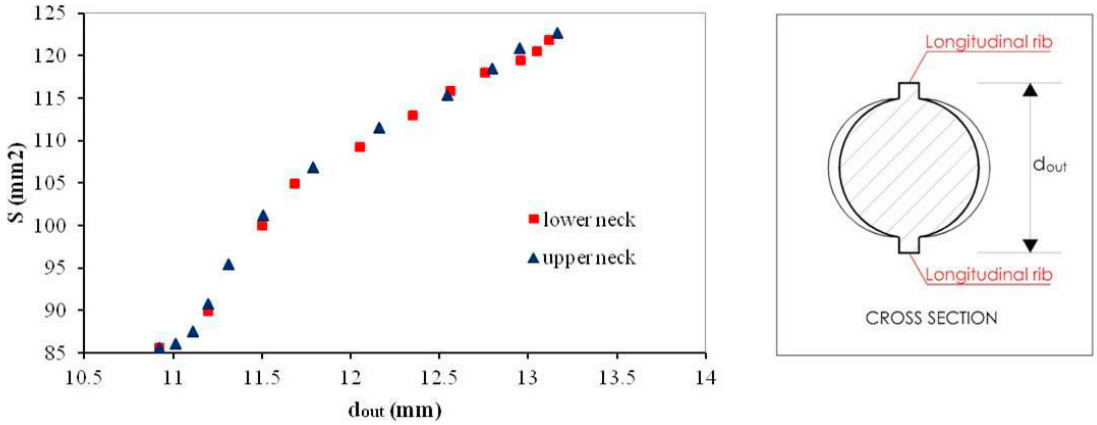

Fig. 4. S vs d_{out} on the neck of a rebar specimen

The evolution of the minimum outer diameter value (d_{out}) was determinated by image processing during the testing, therefore allowing calculating the value of the minimum cross section (S) by Ec. (5) and subsequently the values of ε_{equ} and $\bar{\sigma}_z$ during the necking phase.

For rebar steel, given that Bridgman´s hypothesis (Bridgman, 1944) are not valid, equivalent stress has been calculated according to La Rosa and Mirone (2003) equation, which is not dependent on neck geometry. Results obtained [σ_z (up to onset of necking), σ_{equ} (beyond necking for the minimum cross section)] vs ε_{equ} for one rebar specimen and 5 round ones are shown in Fig. 5. While rebar steel continues under investigation, some conclusions can be raised on comparing both steels behaviour. Round specimens experience necking at lower ε_{gt} value (10.6%) than rebar steel (15.6%). But, on the other hand, the first one reaches a value of ε_{equ} at fracture of 103.8% (±1.8), associated a σ_{equ} of 1067.62 MPa (±11.49), while these values are lower for rebar specimen (41.3%, 825.50MPa).

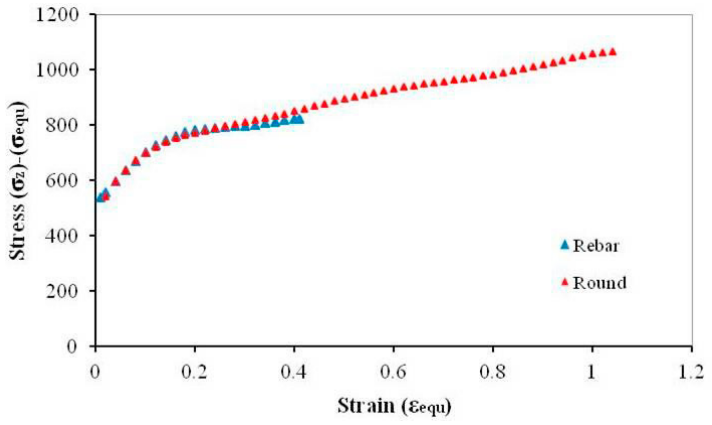

Fig. 5. (σ_z)-(σ_{equ}) *vs* ε_{equ} *for round and rebar specimens*

4. Conclusions and further research subjects

Two types of Tempcore steel have been tested, round and rebar. Short conclusions can be summarized as follows:

- Stress-strain behaviour of both shapes are similar during the homogeneous strain hardening phase. Ribs influence is not detected.
- Bridgman´s hypothesis have been corroborated for round bars but not for rebar ones, which develop no symmetrical necks.
- Ribs decrease the ductility of the steel during the necking phase to cause an earlier failure, which occurs in deformed transversal ribs direction.

As further research subjects, the following items are proposed:

- Analyzing the necking behaviour of a greater number of rebar specimens to increase the experimental data background.
- Making a microstructural analysis of both steels neck area to detect the possible influence of different deformation mechanics.
- Validating the experimental results by FEM (these studies have already been iniciated).

References

Aenor ed., 2006. UNE EN 10080:2006:Acero para el hormigón armado. Acero soldable para armaduras de hormigón armado. Generalidades. Madrid.

Aenor ed., 2011. UNE EN ISO 15630-1: Aceros para el armado y el pretensado del hormigón. Métodos de ensayo. Parte 1: Barras, alambres y alambrón para hormigón armado. Madrid.

Aenor ed., 2016. UNE EN ISO 6892-1: Materiales metálicos. Ensayo de tracción. Parte 1: Método de ensayo a temperatura ambiente. Madrid.

Bridgman, P.W., 1944. The stress distribution at the neck of a tension specimen. Transaction of the American Society for Metals, 32, 553–574.

ASTM, 2009. ASTM E6-09 Standard terminology relating to methods of mechanical testing. West Conshohocken.

Bueno, R., Villegas, D., 2011. Ductility in reinforcing steel: New parameter and applications, Conference Proceedings for the 81st Annual Convention of the Wire Association International. Georgia, USA.

Considére, M., 1885. L´emploi du fer et de l´acier dans les constructions. Annales des Ponts et Chaussées, 6(9), 574–775.

Davidenkov, N.N., Spiridnova, N.I., 1946. Analisis of the state of stress in the neck of a tension specimen. Proceedings American Society for Testing and Materials, 46, 1147–1158.

Donato, G.H., Ganharul, G.K., 2013. Methodology for the experimental assessment for true stress-strain curves after necking employing cylindrical tensile specimens: Experiments and parameters calibration, ASME 2013 Pressure Vessels and Piping Conference. Paris, France.

Eisenberg, M.A., Yen, C.F., 1983. An anisotropic generalization of the bridgman analysis of tensile necking. Journal of Engineering Materials and Technology, Transactions of the ASME, 105(4), 264–267.

Fattah-alhosseini, A., Imantalab, O., Mazaheri, Y., Keshavarz, M.K., 2016. Microstructural evolution, mechanical properties, and strain hardening behavior of ultrafined grained commercial pure copper during the accumulative roll bonding process. Materials Science and Engineering A, 650, 8–14.

Ganharul, G.K., De Braganza Azevedo, N., Donato, G.H., 2012. Methods for the experimental evaluation of true stress-strain curves after necking of conventional tensile specimens: Exploratory investigation and proposals, ASME 2012 Pressure Vessels and Piping Conference. Toronto, Canada.

Gashti, S.O., Fattah-alhosseini, A., Mazaheri, Y., Keshavarz, M.K., 2016. Effects of grain size and dislocation density on strain hardening behavior of ultrafine grained AA1050 processed by accumulative roll bonding. Journal of Alloys and Compounds, 658, 854–861.

Hollomon J. H., Jaffe, L.D., 1945. Tensile deformation. Transactions of the American Institute of Mining Engineers, 162, 223–249.

Rastegari, H., Kermanpur, A., Najafizadeh, A., 2015. Effect of initial microstructure on the work hardening behavior of plain eutectoid steel. Materials Science and Engineering A, 632, 103–109.

La Rosa, G., Mirone, G., 2003. Postnecking elastoplastic characterization: Degree of approximation in the Bridgman method and properties of the flow-stress/true-stress ratio. Metallurgical and Materials Transactions A: Physical Metallurgy and Materials Science, 34(3), 615–624.

Le Roy, G., Embury, J.D., Edwards, G., Ashby, M.F., 1981. A Model of Ductile Fracture Based on the Nucleation and Growth of Voids. Acta Metallurgica, 29, 1509–1522.